

# Optimized Ensemble of Hybrid RNN-GAN Models for Accurate and Automated Lung Tumour Detection from CT Images

Dr. Atul Tiwari<sup>1</sup>, Shaikh Abdul Hannan<sup>2</sup>, Rajasekhar Pinnamaneni<sup>3</sup>, Dr. Abdul Rahman Mohammed Al-Ansari<sup>4</sup>, Prof. Ts. Dr. Yousef A. Baker El-Ebiary<sup>5</sup>, Dr. S. Prema<sup>6</sup>, R. Manikandan<sup>7</sup>

Assistant Professor, Department of Pathology, Government Medical College, Chittorgarh, Rajasthan<sup>1</sup>

Assistant Professor, Department of Computer Science and Information Technology,  
Albaha University, Albaha, Kingdom of Saudi Arabia<sup>2</sup>

Department of Biotechnology, Koneru Lakshmaiah Education Foundation, Greenfields,  
Vaddeswaram, Guntur District-522502, Andhra Pradesh, India<sup>3</sup>

Department of Surgery Salmanyia Hospital Bahrian<sup>4</sup>

Professor, Faculty of Informatics and Computing, UniSZA University, Malaysia<sup>5</sup>

Assistant Professor, Panimalar Engineering College, Chennai<sup>6</sup>

Research Scholar, Vel Tech Rangarajan Dr. Sagunthala R&D Institute of Science and Technology,  
Avadi, Chennai, Tamil Nadu, India-600062<sup>7</sup>

**Abstract**—The early diagnosis and treatment of lung tumour, the primary cause of cancer-related deaths globally, depend critically on the identification of lung tumours. In this approach, a new method is suggested for detecting lung tumours that combines a Gaussian filter with a hybrid Recurrent Neural Network-Generative Adversarial Network (RNN-GAN). Utilising the sequential data seen in images of lung tumours, the RNN-GAN architecture is used. In processing the sequential input, the RNN component looks for temporal relationships and patterns. The GAN component improves the training of the RNN for accurate classification by creating synthetic tumour specimens that resemble actual tumour images. In addition, the proposed approach pre-process lung tumour images using a Gaussian filter to improve their quality. The Gaussian filter improves feature extraction and the visibility of tumour borders by reducing noise and smoothing the pictures. The proposed experimental findings on a dataset of lung tumours shows that the suggested strategy successful. In comparison to conventional techniques, the hybrid RNN-GAN delivers higher accuracy in lung tumour identification due to the incorporation of the Gaussian filter. While the GAN component creates realistic tumour samples for improved training, the RNN component efficiently captures the sequential patterns of tumour images. The lung tumour images are pre-processed using a Gaussian filter, which greatly enhances image quality and facilitates precise feature extraction. The proposed hybrid RNN-GAN with the Gaussian filter shows promising potential for accurate and early detection of lung tumours. The integration of deep learning techniques with image pre-processing methods can contribute to the advancement of lung cancer diagnosis and treatment, ultimately improving patient outcomes and survival rates. Further research and validation are necessary to explore the full potential of this approach and its applicability in clinical settings.

**Keywords**—Lung tumour; recurrent neural network; generative adversarial network; CT images; hybrid

## I. INTRODUCTION

Lung cancer has become one of the main causes of cancer-related death in many countries all through the world. According to data on cancer worldwide, a startling number of new diagnoses and fatalities in 2018 were caused by lung cancer. There were a total of 1,761,007 fatalities, representing 18.4% of all tumour-related fatalities, and 2,093,876 newly identified instances, or 11.6% of all cancer sites [1]. The term "lung cancer" describes the unchecked proliferation of cancer cells in the lungs, which raises both male and female mortality rates. While it cannot be totally prevented, there are some measures to lessen the risk of this illness, which is characterised by the fast proliferation of lung cells. For patients to have a better chance of surviving lung cancer, early identification is essential [2]. Lung cancer can be found via diagnostic imaging tests. Complex lung cancer datasets are examined to discover essential features using machine learning (ML) methods. A CAD method was created in the early period to help clinicians analyse medical pictures in an effort to increase effectiveness and the rate of survival. Healthcare has greatly benefited from a variety of machine learning methods. Additionally, we have investigated deep learning approaches, methodologies, and algorithms that may be used for identifying, detecting, and forecasting various cancer kinds [3].

Pathologists may be helped by the application of CNN-based approaches in the identification of lung cancer [4]. Selvanambi et al. recommended a more complex recurrent neural network that was optimised via glow-worm swarm optimisation to present a unique method for predicting lung cancer [5]. The use of computed tomography (CT) as a diagnostic tool for pulmonary disorders has become more important. Particularly, columnar CT is widely regarded as helpful tools in the diagnosis of scattered interstitial lung disease (DILD) images have been the subject of several

researches aimed at improving computerised analysis of images and computer-aided diagnostic (CAD) systems. These developments are meant to increase the precision and efficacy of pulmonary disease diagnosis across the board, including diffuse interstitial lung disease (DILD) [6]. With the advancement of computer-assisted diagnosis and detection techniques, several efforts are being made to improve the clinical effectiveness of lung cancer detection and categorization. Sajja et al. [7] advised deep learning and transfer learning to detect lung cancer. Their study demonstrates how effective this method is in accurately identifying lung cancer cases. Bhatia et al. [8] presented a feature extraction strategy based on deep residual networks for the identification of tumours. Tulin Ozturk, et al. [9] suggested a model using deep learning for automating tumour diagnosis.

The American Cancer Society estimates that every year, between 10 and 20 percent of all cancer patients (or around 1.7 million people) receive incorrect diagnoses, as well as that at least 40,000 of these individuals end up dying as a direct result. Furthermore, cancer is the second-leading cause of mortality in the US. There is a chance of making a mistake when a pathologist has, on a typical basis, 80 Computed Tomography (CT) slides each patient to assess. Therefore, it is necessary to computerise the tumour diagnosis procedure in order to cut down on the possibility of human mistake. Monitoring with low-dose CT, which has been demonstrated to lower lung cancer mortality by up to 20%, has the potential to identify lung cancer at an earlier stage. However, diagnosing a lung CT scan is a highly specialised process needing specialist understanding. If done manually, it is a difficult and time-consuming process. False negative situations occur when a cancer manages to escape detection by the human eye since it may resemble other lung-existing particles in terms of size and texture. The current study primarily focuses on the qualitative examination of a cancer that a pathologist manually found during a single CT scan. The literature lacks a completely automated framework that can automatically detect tumours across a series of CT scans in a single run, giving the viability of the framework priority. Despite this, there would be 28.40 million new instances of tumours worldwide in 2040, a 48 percent rise from the previous year. An increase in risk factors, such as smoking, will make (even worse) people with respiratory issues, people who have been smoking for 30–40 years, patients who experience no symptoms, as well as patients with no symptoms are common hurdles in identifying lung tumours in patients from the decade. In an effort to overcome the difficulties involved in the diagnosis of tumours, various investigators have employed a variety of strategies, such as differentiation, recognition, and classification methods [10].

Using a Gaussian filter, the picture is first enhanced by data pre-processing, and the noise in the CT representation is then eliminated. The pre-processing methods divide the incoming data into several categories. Pre-processing will be followed by the extraction of the afflicted lung region. The afflicted area of the lung tumour is found using segmentation. The segmentation of the CT representation facilitates the extraction of useful characteristics for the procedure. To prepare the input image for testing and training, two sets are

divided. During training and testing, the errors in the samples of data are removed. Then, using the feature extraction process, which extracts the features using the Grey Level Co-occurrence Matrix (GLCM), the cancerous lung nodule is found. The RNN-GAN hybrid model is used to distinguish between the damaged and unaffected parts of the lungs.

The following are the research's main contributions:

- From a lot of cases, CT pictures are initially gathered.
- In addition, undesirable noises are present in the reconstructed real CT lung pictures, which are filtered using a sophisticated Gaussian filter model.
- The segmentation procedure has been carried out using an enhanced K-means clustering.
- The Grey Level Co-occurrence Matrix (GLCM) was used to extract features.
- The afflicted and unaffected lung nodules are categorised by the RNN-GAN.
- To demonstrate the usefulness of the implemented technology, its performance is verified and compared to current methodologies.

The manuscript of the approached paper is organised as follows: In Section II, some related works are reviewed. In Section III, Information regarding the problem statement is provided. In Section IV, the proposed RNN-GAN is covered in detail. In Section V, experiment results are provided, and discussed, and an extensive evaluation of the proposed approach to current best practices is made. In Section VI, the conclusion of the paper is provided.

## II. RELATED WORKS

Rahman et al. [11] utilized several open datasets to construct a database comprising 3500 chest X-ray images infected with TB and 3500 images of healthy chests. They developed a reliable method for consistently identifying tuberculosis from these chest X-ray images. Image initial processing, enhancement of data, segmentation of images, and deep learning techniques classification algorithms were all used in the methodology. The success of a transfer learning strategy employing deep CNN for automatically detection of tuberculosis is discussed in conclusion. The study assessed nine various CNN models and found that the ChexNet model performed well (96.47%, 96.62%, and 96.47%) without image segmentation, while the DenseNet201 model excelled with (98.6%, 98.57%, and 98.56%) segmented lungs. The study also emphasized the significant improvement in classification accuracy through image segmentation. The Score-CAM visualization results provided confirmation of the key role played by lung segmentation in ensuring accurate decision-making based on the lung region. One potential drawback of the proposed method is that it focuses only on the detection of TB without considering the detection of other lung abnormalities or diseases. While this approach is valuable for TB detection it may not be suitable for identifying other lung conditions or providing a comprehensive analysis of the patient's chest radiograph.

Bharati, et al. [12] proposed a new deep learning hybrid framework by merging (STN) VGG with CNN and named as VDSNet to detect the lung disease. The dataset obtained from the Kaggle library was subjected to this methodology. There are a sizable number of lung X-ray pictures in the investigation's dataset. This model has the greatest validation accuracy of 73% for the complete dataset example. Comparatively, the accuracy of the validation values for various other models, are 69%, 67.8%, 60.5%, 69.5%, and 63.8%, respectively. With an accuracy for validation of 73%, this framework outperformed the sample dataset's efficiency of 70.8%. However, VDSNet requires more time for training, with the process taking 431 seconds as opposed to the sample dataset's 19 seconds.

Asuntha & Andy Srinivasan [13] focuses on using Deep Learning methods to locate cancerous lung nodules and classify lung cancer severity. Fuzzy Particle Swarm Optimisation Convolutional Neural Networks (FPSOCNN) is a unique method that is suggested for lowering computational complexity. We use a number of feature extraction methods, such as HoG, wavelet transformations, LBP, SIFT, and Zernike Moment. The FPSO algorithm is used to extract texture, geometric, volumetric, and intensity characteristics and choose the best feature; evaluation utilising a unique dataset (DICOM) from the Indian hospital Aarthi Scan. Nearly 10,000 lung pictures are included. All images have a resolution of 256 by 256. The experimental data demonstrate that new FPSOCNN outperforms existing methods. The optimisation and classification performance of the suggested model still require work. This suggests that the suggested paradigm could have some drawbacks.

Kim et al. [14] employed a technique called transferred learning to elevate the accuracy and efficacy of CAD and created a deep learning approach for classifying lung disease in chest X-ray (CXR) images. The method used CNN models, particularly the Efficient Net v2-M model, as well as the transfer learning techniques, empirical hyper-parameters, and CNN models. The one-step, end-learning method utilised to gather useful features for sickness categorization involved simply feeding raw CXR images into the deep learning system. Two datasets were used for the experiments, which include a privately created database with four categories and an open-access benchmark dataset from the U.S. National Institutes of Health with three distinct groups. The suggested strategy produced reliable results in precisely classifying lung diseases. The suggested method's disadvantage is that the success rate for the different categories varied, with the usual categories having the lowest possible accuracy at 63.60%. This suggests that in comparison to the other lung disease categories, the model would have trouble properly classifying normal patients.

Demir et al. [15] a range of sample frequency ranges, noise from the background, and other noises are included in the CBHI 2017 database, which was suggested. The lung sound waves were transformed into spectrogram visualisations. Two methods based on deep learning were used to classify lung sounds. In the first approach, lung sounds were categorised using an SVM classifier, and features were retrieved using an already trained CNN. In the second technique, the previously

trained deep CNN model was modified by transfer learning while lung sounds were identified using spectrogram images. The accuracy of the first and second suggested approaches was 65.5% and 63.09%, respectively. This strategy is then demonstrated to perform better than other results by comparison to the current results. The problematic elements in the suggested approach for classifying lung sounds include noises, background noise, and different sampling frequencies. This suggests that a smaller dataset may have been used to test the model.

Shakeel, et al. [16] focuses on boosting the accuracy of lung cancer detection and the quality of lung pictures. The (CIA) dataset's lung CT pictures were used. A weighted mean histogram equalisation method was used to minimise misclassification and improve picture quality by removing noise from the photos. Further enhancing picture quality, the afflicted region was segmented using an IPCT. A deep learning neural network was instantly developed to anticipate lung cancer using the partitioned region's multiple spectral properties. The technique achieved a success rate of 98.42% with a low classification error of 0.038, and its effectiveness was assessed using MATLAB-based simulation results. These results show how well the algorithm performs in correctly identifying lung cancer and enhancing lung pictures. It is noted that without data enhancement and transfer learning, categorising numerous lung illnesses on grayscale chest X-ray (CXR) pictures is difficult. A trade-off exists when dropout regularisation is used among overfitting and losing important information. A low rate of abandonment might result in acceptable performance on the initial training set but poor performance on the validation or testing set, whereas a large dropout rate could result in the loss of critical features.

Chen, et al. [17] proposed to assess chest X-ray pictures of common pulmonary diseases in children. A computer-aided diagnosis method has been created. The appropriate lung field is automatically recognised and cropped by the algorithm using the YOLOv3 architecture. The one-versus-one classification system outperformed the other two when they were compared to each other. In recognising certain illnesses and detecting irregularities, the system had great accuracy rates. The suggested method's limitation to useable medical resources is its main flaw. Issa, et al. [18] examined how well four pre-trained participants performed using CXR pictures to identify various lung illnesses. Utilising CXR pictures and 5-fold cross validation, the model was trained and evaluated. With a remarkable area under the curve (AUC) of 99.84% for ROC, XceptionNet had the greatest accuracy (94.775%). With regards to accuracy, quick convergence, resource use, and almost real-time detection (0.33s), DarkNet19 demonstrated an excellent balance. With a lengthier prediction time (5.68s), the ensembles feature technique, which included many models, obtained the maximum accuracy of 97.79%.

### III. PROBLEM STATEMENT

The problem addressed in the research is the development of a deep learning-based CAD system for classifying lung diseases in CXR images, with the ultimate aim of enhancing diagnostic accuracy and efficacy in medical imaging [14]. The database contains a range of sample frequency ranges,

background noise, and other noises, making lung sound classification challenging. The researchers sought to develop effective methods based on deep learning to classify these lung sounds accurately [15]. In this proposed approach a unique method for Optimized Ensemble of Hybrid RNN-GAN Models for Accurate and Automated Lung Tumor Detection from CT Image.

#### IV. PROPOSED RNN-GAN

By incorporating RNN-GAN, the proposed method effectively leverages the sequential nature of lung tumour, capturing temporal patterns that may be crucial for accurate tumour identification. The GAN component plays a vital role in creating synthetic tumour samples, improving the training process, and augmenting the limited dataset to better handle class imbalances and improve classification accuracy. The application of the Gaussian filter enhances image quality and reduces noise, leading to improved feature extraction and better visibility of tumour borders, ultimately contributing to

more reliable and precise tumour detection. The combination of deep learning techniques with image pre-processing methods shows promise for early detection of lung tumours, which is critical for improving patient outcomes and survival rates. The proposed method represents a significant step in the field of lung cancer diagnosis and treatment, demonstrating the potential of integrating cutting-edge techniques for addressing complex medical challenges.

The computerised tomography representations of lung tumours are first gathered. The simulations are then used for teaching and testing. The Gaussian filter is applied in the pre-processing of lung-dependent CT images to remove extra noise. In this work, lung nodules are first detected using a mixed RNN-GAN model. The severity of lung nodules is categorised using the suggested RNN-GAN model. Fig. 1 shows the RNN-GAN model.

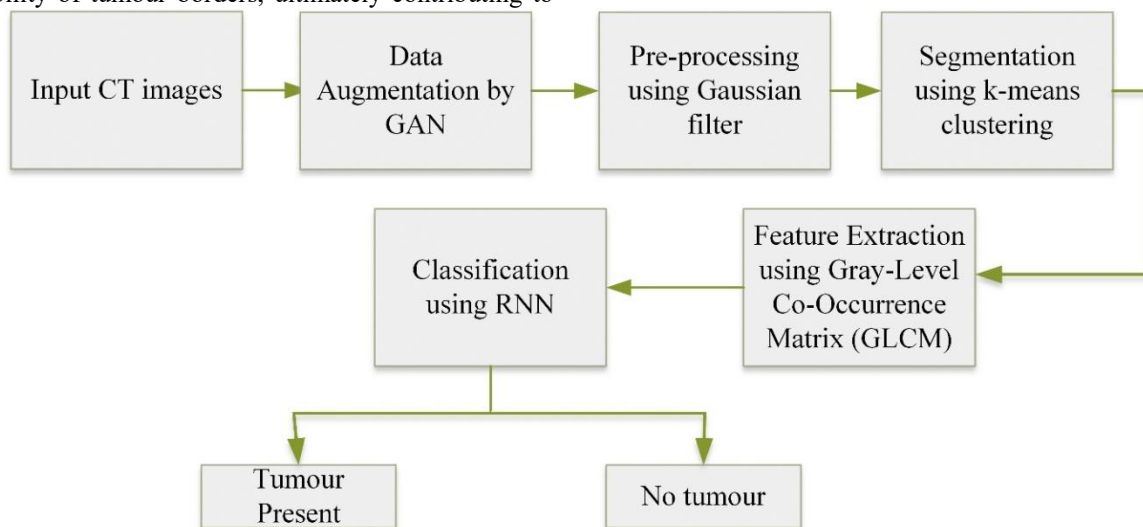


Fig. 1. Proposed RNN-GAN model.

#### A. Data Collection

CT lung representations of 10,000 datasets containing healthy and unhealthy lung representations collected from the University of California are utilized in the research. Among these 50% of representations are used for training and 50% of representations are utilized for testing [20]. The assessed system was tested using many cancer datasets from the University of California, Irvine collection. The data set has 57 high points, but only four of them may be looked at with conventional analysis of components. The lungs dataset was utilised in evaluating their programmed method for cancer identification. There are 32 occurrences, 57 features, and a single class characteristic altogether in the collection. The dataset, which consists of 32 samples with a total of 57 characteristics and a theoretical range of 0–3, was found in the database for machine learning at UCI. Here 2500 is a tumour data. The collected datasets are given in Table I.

TABLE I. COLLECTED DATASETS

	Unhealthy	Healthy	Overall
Training data	2500	2500	5000
Testing data	2500	2500	5000

#### B. Data Augmentation

The data augmentation technique creates augmented training data using a style-based generative adversarial network (GAN). It makes sense to utilise data augmentation techniques to address the issues of data imbalances and scarcity. This strategy has shown to be a successful means of enhancing model performance and avoiding overfitting. Utilising GAN to enhance data or create training samples is another genre. The GAN training phase and enhanced image generation are the two components of this approach. The design of the generator and the discriminator are both optimised concurrently throughout the training phase. They are instructed to use both the semantic label and the style matrix to rebuild the actual image [21].

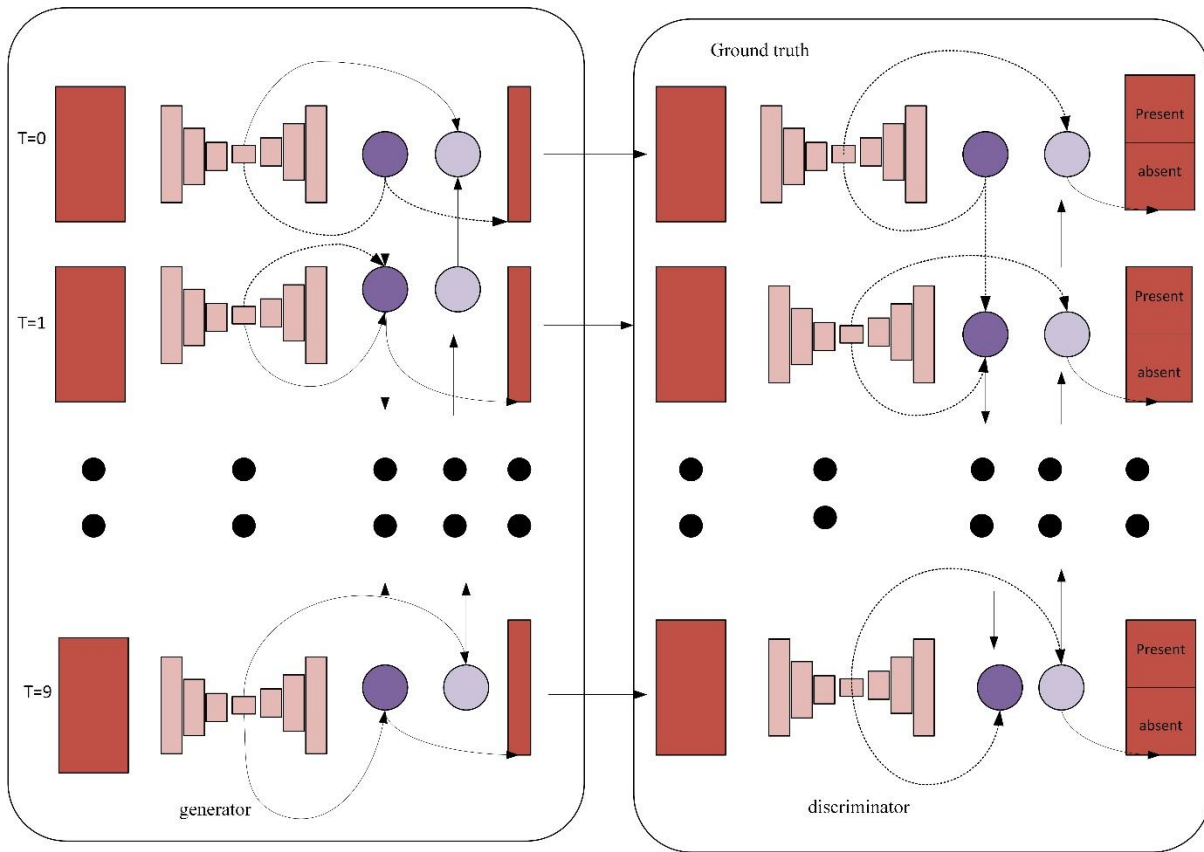


Fig. 2. Architecture of RNN-GAN.

A generating network (G) and a discriminative network (D) are the two deep networks that make up the RNN-GAN's architecture, which is shown in Fig. 2. As a condition, G produces a series of 2D segmentation semantic outputs from a set of 2D images, and D determines whether or not those outputs are real. RNN-GAN experiences improvements where better resolution attributes are coupled with upsampled relatively not high-quality image attributes, helping the neural network to learn both global and local data. Typically, a GAN's generative model G aims to translate the output image  $v$  into the erratic noise vector  $z$ ;  $G: z \rightarrow y$ . The possibility that a sample comes from the source of data  $x$  false as opposed to its data for training  $x$  genuine is calculated by a model exhibiting bias  $D$  in the meanwhile. More specifically, an RNN-GAN network is proposed, and a generative model learns its semantic classification of matching labels from a set of 2D medical images  $u_i, v_{i_{seg}}$ ;  $G: u_i, z \rightarrow \{v_{i_{seg}}\}$ . The discriminator uses the ground truth and the generated data to assess if the label that was predicted is true or false whereas the segmentation was anticipated at the pixel level by the generator which is represented in eq. (1).

$$\mu_{adv} \leftarrow \min_G \max_D k(G, D) = K_{U, v_{seg}} [\log D(u, v_{seg})] + K_{u, z} [\log(1 - D(u, G(u, z)))] \quad (1)$$

### C. Pre-Processing

The initial step in finding cancerous pulmonary nodules is pre-processing. It is used to remove unnecessary data in addition to fill in dataset gaps. The peculiar and abnormal

vibrations that influence the CT portrayals slow down the rate of evaluation of the first visualisations. The CT depictions are most affected by the irregular noises that are caused by internal and external causes. As a consequence, the noise in CT lung depictions is reduced using the resulting Gaussian filter. The created Gaussian filtering technique is used to minimise residual deviations of spatial severity in the depictions as well as disturbance in the representations. The use of the filter known as the Gaussian causes the mean value of the surrounding pixels, which depends on the distribution of Gaussian, substitutes the distorted pixel within the representation. The RNN-GAN model makes use of noise-reduced representations to identify lung cancer nodules [22]. The Gaussian function is given in eq. (2).

$$G(V) = \frac{1}{\sqrt{2\pi\delta^2}} e^{-\frac{v^2}{2\pi\delta^2}} \quad (2)$$

Where  $\delta$  is the standard deviation of the distribution. The distribution is assumed to have a mean of 0.

### D. Segmentation Using K-Means Clustering

The segmentation approach is mostly used for separating the impacted area in illustrations based on CT images. For image processing to be implemented, the segmentation procedure must be accurate. Segmenting an image is frequently used to determine the location of the affected nodules as well as the constraints of the images' curves and lines. The representations are divided into groups of pixels, and each group's pixels are annotated. Classification of cancer

nodules and the generation of sufficient data to perform additional identification are the primary goals of picture segmentation in medical representation processing. The technique of dividing a picture into several sections, each with a different collection of pixels, is known as image segmentation. The method of global thresholding technique depends on the gray-level pixels' luminosity for threshold P, projected to divide the picture. Using eqn. (3) and  $I(u, v)$ , it is possible to describe the fragmented picture that was obtained by global thresholding. The image's pixel value is represented here by  $t(u,v)$ .

$$I(x, y) = \begin{cases} 1 & \text{if } I(u, v) > P \\ 0 & \text{if } I(u, v) \leq P \end{cases} \quad (3)$$

By implementing a certain structural element at every site that is feasible for smoothing the region of interest, quantitative morphological procedures are estimated. When F is a binary picture and J is an organising element, as shown in eqns. (4), (5), (6) and (7), respectively, mathematical computations are carried out.

$$\text{Erosion} : L \ominus J = \{H | (J_A \subseteq L)\} \quad (4)$$

$$\text{Dilation} : F \oplus J = \{H | (J_A \cap L \neq 0)\} \quad (5)$$

$$\text{Opening} : F \ominus J = L \ominus J \oplus LJ \quad (6)$$

$$\text{Closing} : F \ominus J = L \oplus J \oplus LJ \quad (7)$$

The simplest and most traditional method of analysing clusters is the k-mean clustering algorithm. To divide the provided dataset through two or more groups, k-means is used. Since choosing the right cluster core is crucial for obtaining the most beneficial results, the correctness of the procedure is assessed by examining every single cluster centre that the algorithm generates. The Euclidean distance, that is employed to assign pixels to certain clusters, is a pretty straightforward technique for separating the dataset. This algorithm makes use of the following function as represented in eq. (8).

$$k = \sum_{i=1}^r \sum_{j=1}^s V_{ij} \|u^i - \gamma_s\|^2 \quad (8)$$

Where,  $V^i$  is the number of data points for the  $i$  th cluster,  $u^i$  is the number of pixels,  $v^j$  is the cluster centres,  $\|u^i - \gamma_s\|$  is the Euclidean distance between  $u^i$  and  $v^j$ , and  $C^i$  is the number of cluster centres. In the anticipated phase, points of information are allocated to the nearest cluster. Each cluster's kernel is determined during the optimisation process [23].

#### E. Feature Extraction

In order to record and retain the details of the initial collection of data, the process of separating characteristics requires turning unorganised information into quantitative attributes. Each patient has a unique way of processing information, and these characteristics are derived from the full collection of depictions that were taken. The number of dimensions of the depiction must be lowered for the purpose to detect lung nodules while the dimension of the representation grows throughout testing. To fix this problem, the extraction of features is done. The Grey Level Co-occurrence Matrix (GLCM) is used in the feature extraction. By computing various combinations of pixels with specific

values, it shows how the visual representation is organised hierarchically. The GLCM employs the associated grayscale and displays the luminosity of the depicted pixels. To remove the statistically important texturing characteristic, the second-degree representation's energy, contrast, correlation, entropy, homogeneity and other qualities are assessed.

The extraction of features stage is carried out using the GLCM technique based on the scenario. The GLCM functions determine how frequently pairs of pixels with specific parameters and in a particular arrangement of pixels appear in an image in order to describe the surface texture of that image. statistical variables generated from the following GLCM outcomes. The formulas below were used to determine these values:

1) *Energy*: When the total values are asymmetrical and usually greater, energy is defined as the presence of an equal number of grey levels in portrayals. eqn. (9) calculates the energy of the provided data.

$$E = \sum_o \sum_p \{Q(o, p)\}^2 \quad (9)$$

Where the representations are denoted as Q and gray level squares are denoted as (m, n).

2) *Contrast*: Attributes are used to assess the local contrasts of a representation, so if it is in a consistent saturation value, it is assessed as a low value. The number of grayscale values in the original form as well as the contrast are projected in eqn. (10)

$$C = \sum_{y=0}^{Rs} y \{ \sum_{o=0}^{Rs} \sum_{p=1}^{Rs} Q(o, p) \} \quad (10)$$

Where R indicates the gray level of the representation, Q indicates the representation, and (o,p) indicates the gray level square of the representation.

3) *Correlation*: The relationship between the features can be used to account for both the linear dependence of the grey levels on the pixels and statistical interactions between the parameter values. The characteristics are exposed in eq. (11).

$$C = \frac{\sum_o \sum_p (o,p) Q(o,p) - \delta_x \delta_y}{\sigma_x \sigma_y} \quad (11)$$

In the representation, the values of mean, as well as standard deviation, are  $\delta_x$ ,  $\delta_y$ ,  $\sigma_x$ , and  $\sigma_y$  are defined as row and column.

4) *Entropy*: The anticipated significant amount of the uncertainty of the split of the grey levels is known as entropy. which is denoted in eq. (12) [24].

$$E_n = - \sum_o \sum_p Q(o, p) \log_2(Q(o, p)) \quad (12)$$

5) *Mean*: Mean indicates the overall brightness within the matched image. It has very limited expressive and discriminating skills which is denoted in eq. (13).

$$M = \sum_{i=0}^Q \frac{i_r^{mi}}{\sum_{i=0}^Q \frac{mi}{M}} \quad (13)$$

Where, M=total number of pixels, mi= number of pixels in level i

6) *Energy features*: Angular second instant is another name for energy. The grey level occurrence matrix's sum of squared elements is returned. Energy for a constant picture will be 1 and it is denoted in eq. (14)

$$E = \sum \sum Q(o, p)^2 \quad (14)$$

7) *Homogeneity*: It evaluates how well the GLCM's constituent distribution matches its diagonal. Which is denoted in eq. (15) [25].

$$H = \sum_{i,j} \frac{Q(i,j)}{1+||i-j||} \quad (15)$$

#### F. Classification using RNN-GAN

In order to reduce the total distinction amongst the anticipated value and the biggest value already in existence, the loss caused by opposition with 1 distance is used. The small quantity is made up of 2D pictures taken from an identical patient using the identical acquisition surface during the stages of training and testing. Both the variance and the mean are estimated for an individual from the exact same acquisition plane as well as similar phase, and then the recommended method first normalises the inputs from all available photos. The impact of anomalies is reduced because to this normalisation. The recommended method utilised batch standardisation to equalise the signals that were employed (activations from the previous layer) coming into every layer specified in eqns. (16) and (17) using the mean and variance of all the activation for the entire mini-batch. There is less turbulence and the borders are smoother since the parameter function takes into account RNN features and differences between expected and actual segmentation.

$$\mu_1 = K_{u,z} ||vseg - G(u, z)|| \quad (16)$$

$$\mu_2 = \frac{1}{d} \sum_{i=1} \sum_{j=1} \frac{v_{i,seg} \cap G(u_{ij}, z)}{v_{i,seg} \cap G(u_{ij}, z)} \quad (17)$$

where u and z represent, correspondingly, the quantity of 2D slices and the degree of semantic classes for every patient. Additionally, the suggested method combined categorised loss of accuracy, to reduce unbalanced data from training by allocating a greater cost to a fewer-represented group of pixels, raising its value throughout the learning process. Classification accuracy loss determines if the maximum real value and maximum forecasted value for each classification category are equal. The final of RNN is calculated through eq. (18) [26].

$$\mu_{RNN}(D, G) = \mu_{adv}(D, G) + \mu_1(G) + \mu_2(G) \quad (18)$$

In traditional generative modelling approaches, the performance of a model is indicated by the reverse divergence between the desire distribution  $Q_r$  and our generator's distribution  $Q_s$  as represented in eq. (19).

$$V_{kl}(Q_r || Q_s) = \int x Q_r \log \frac{Q_r dx}{Q_s} \quad (19)$$

RNN-GAN is a mixture of the RNN and GAN, two well-known deep learning models. While GANs are used to produce accurate patterns of distribution, RNNs are utilised for processing data sequentially. RNN and GAN frameworks should be combined for cooperative training. Actual and false lung tumour pictures produced by the GAN are used to train the RNN. The RNN gains the ability to distinguish between benign and malignant pictures. Utilise the test set of lung tumour pictures to assess the trained RNN model's performance. The proposed approach need to alter the RNN-GAN model's hyper-parameters, architecture, or data augmentation strategies in accordance with how well it performs. The goal of this stage is to increase the model's generalisation and consistency capabilities.

Fig. 3 represents the proposed flow diagram for lung tumour detection. Initially the data is loaded. The images pre-processed by Gaussian filter to remove the noise present in the image. The pre-processed image is segmented using k-means clustering technique. Then the features are extracted by GLCM technique and finally the proposed classifier classifies the tumour.

---

#### Algorithm: RNN-GAN mechanism

---

**Input:** CT representation of lung nodules

**Output:** Detection of affected and unaffected lung nodules

Load input representation data

Train the input images  $v_i$  in the system, where  $i = 1$  to  $n$

Pre-processing of images

Let  $U(i)$  be the input images from the dataset

for every  $U_i$  // Gaussian filter

// V denotes

$V_v(i) = V(i) - N$  // unwanted noise

Segment the affected part

// Bat and Whale Optimization

Initially, the affected part is detected

If( initial region is met)

Update the tumour present

Else

Find the initial location

Repeat until the stopping condition is reached // until all the tumour region is identified

End if

End if

Return

Feature extraction using

GLCM

Classification of tumour

//RNN-GAN

classifier

---

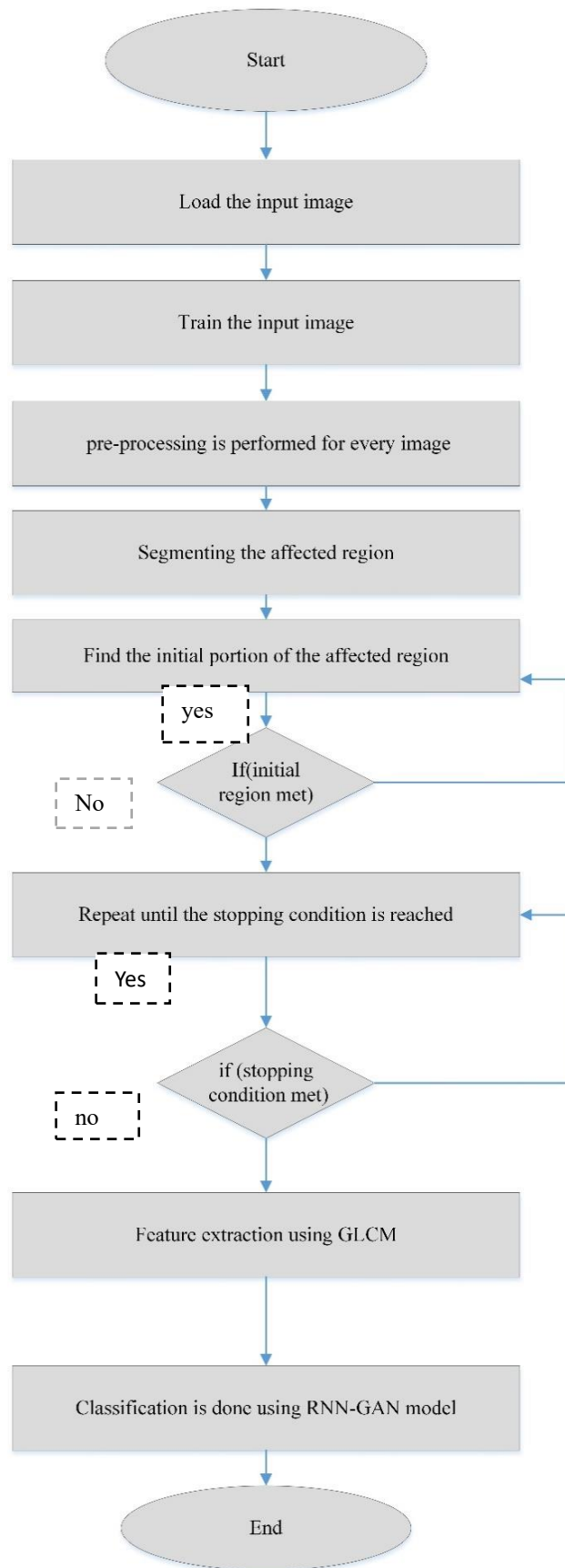


Fig. 3. Flow diagram of the proposed model.

V. RESULT AND DISCUSSION

The recommended method has been evaluated using lung computed tomography datasets and executed in MATLAB software on the Windows 10 platform. The combination of revolutionary RNN-GAN is used to detect a lung tumour when contrasting datasets from healthy and unwell individuals. Performance indicators like Accuracy, Precision, Recall, and F-measure are used to evaluate the effectiveness of proposed methodology.

The proposed model will be implemented using the python programming language. The test is run on a machine equipped with an Intel(R) Core(TM) i5-3470 CPU @ 3.20 GHz, 3200 MHz, 4 core(s), 4 logical pro. And micro software 10 pro, a micro soft corporation, is an OS manufacturer installed physical memory (RAM) 8GM.

A. Accuracy

The model's complete precision demonstrates how well it functions throughout every classification. In general, it is the notion that all occurrences will be accurately predicted. Eq. (20) expresses accuracy.

$$A = \frac{T_{pos}+T_{neg}}{T_{pos}+T_{neg}+F_{pos}+F_{neg}} \quad (20)$$

B. Precision

The number of exact positive ratings that differ from the total number of positive evaluations is used to calculate precision. Eqn. (21) is used to compute the portion of precisely identifying the afflicted area as having tumour nodules.

$$P = \frac{T_{pos}}{T_{pos}+F_{pos}} \quad (21)$$

C. Recall

The recall is the correlation between the overall quantity of accurately classified samples that are positive and the number of true positives. It displays the percentage of predictions that correctly identified the malignancy nodules that is given in eq. (22):

$$R = \frac{T_{pos}}{T_{pos}+F_{neg}} \quad (22)$$

D. F1-Score

The F1-Score computation combines precision and recall. Precision and recall are used to construct the F1-Score given in eq. (23):

$$F = \frac{2 \times \text{Precision} \times \text{recall}}{\text{Precision} + \text{recall}} \quad (23)$$

TABLE II. PERFORMANCE EVALUATION

	CNN	RNN-GAN
Training	99.1	99.8
Testing	97.5	98.9

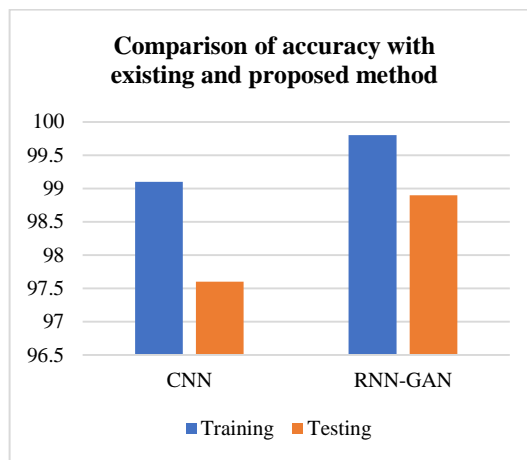


Fig. 4. Accuracy comparison for existing and proposed method.

The accuracy of the convolutional neural network used for both the training and testing stages is 99.4% and 97.6%, respectively, according to Table II. When RNN-GAN is utilised, the accuracy of the testing and training processes increases to 99.8 and 98.9, respectively. Fig. 4 shows an evaluation of performance.

TABLE III. COMPARISON OF ACCURACY

Classifier	Accuracy
CNN [10]	89.8
FPSOCNN [12]	98.9
SVM [15]	97.2
SVM +CNN [14]	97.5
Proposed RNN-GAN	98.6

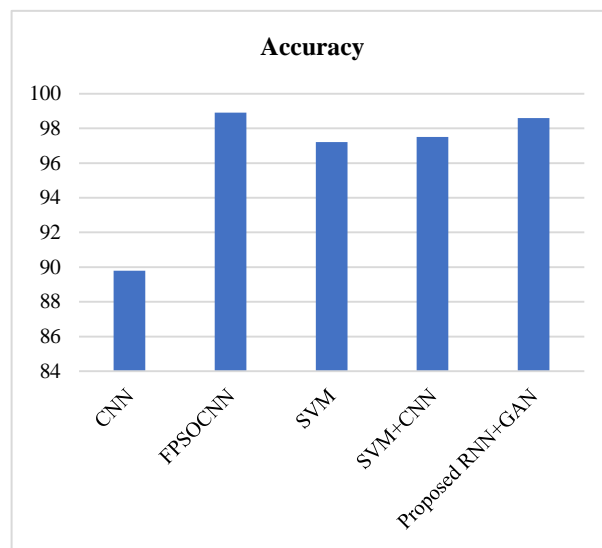


Fig. 5. Comparison of accuracy.

When compared to the current lung tumour detection techniques, the suggested technique RNN-GAN obtains a greater level of accuracy. The contrast of efficiency between RNN-GAN and other approaches is shown in Fig. 5 and Table III.

TABLE IV. COMPARISON OF PRECISION AND RECALL

	Precision	Recall
MLP classifier	88.5	86.9
CNN	95.9	98
SVM and CNN	98.9	92
RNN-GAN	100	99

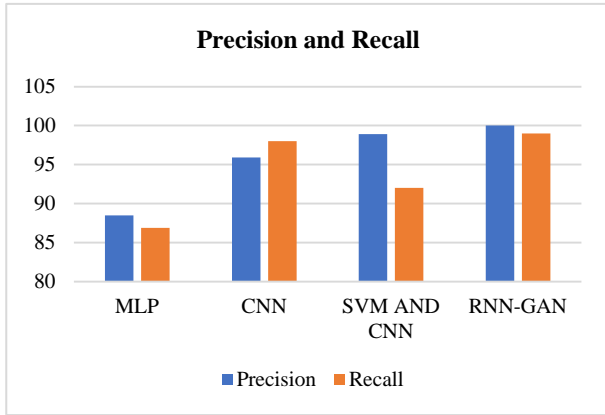


Fig. 6. Comparison of precision and recall.

Table IV demonstrates that the proposed technique of combined RNN-GAN achieves higher precision and recall of 100% and 99% when compared to the existing lung tumour nodule detecting methods the advanced RNN-GAN gives better accuracy than the performance evaluated. Here, the achieved accuracy level is 98.92% using the RNN-GAN model. Fig. 6 illustrates the precision and recall between RNN-GAN and other methods.

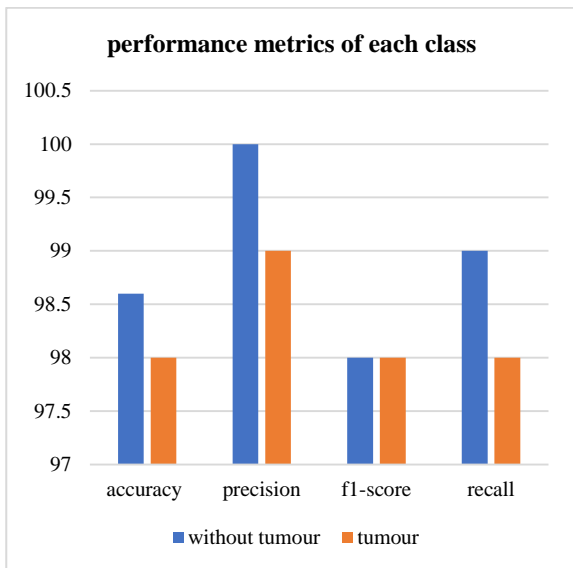


Fig. 7. Performance metrics of each class.

In Fig. 7, the performance metrics for each class are presented. The analysis involves two classes: "without tumour" and "tumour." The metrics include accuracy (98.6%), precision (100%) for "without tumour," and accuracy (98%), precision (99%) for "tumour." Additionally, the f1-score and

recall values for both classes are provided, indicating the model's overall classification performance for each category.

## VI. CONCLUSION

Today's healthcare technology is rapidly advancing image processing, but in some cases, the intricate nature of the depictions makes it difficult to categorise and diagnose disorders. The ill or damaged section is classified, characterised, and segmented using the indicated method. It mainly focuses on locating lung tumour nodules. First, data from patients with various types of lung tumours are acquired from their CT scans to learn more about the patient. The unexpected effects or distortion in the images from CT are then removed employing a Gaussian filter that is applied during pre-processing. The RNN-GAN framework is utilised for scenarios including the recognition of lung cancers. The RNN-GAN architecture enables sequential processing of lung cancer pictures and the creation of realistic tumour samples by combining the strengths of RNNs and GANs. Because the data are sequential, the RNN component of the RNN-GAN can accurately classify the lung tumour images by detecting relationships between time and patterns. The RNN can use the synthetic tumour samples produced by the GAN component to train and improve its capacity to distinguish between benign and malignant tumours. The RNN-GAN architecture learns to categorise lung tumour images through joint training using both actual and produced tumour samples. While the GAN creates realistic tumour samples to aid in learning, the RNN is taught to categorise the photos. The RNN-GAN strategy has the potential to increase the precision and effectiveness of lung cancer detection systems by utilising the complementary capabilities of sequential data processing provided by RNNs and generative modelling provided by GANs. To guarantee the success of the RNN-GAN framework for lung cancer detection tasks, it is crucial to take into account the unique implementation aspects, such as architectural choices, training methods, and dataset quality. The proposed method requires careful evaluation on larger and diverse datasets to ensure generalization to various tumour types and patient populations. Additionally, the computational cost of using RNN-GAN and Gaussian filters may be a challenge for real-time applications; optimizing the model's efficiency is a critical aspect for future research and practical deployment. To validate and perfect the RNN-GAN technique for practical lung tumour detection applications, more investigation and testing are required. Consequently, this model's forecast precision was 98.6%.

## REFERENCES

- [1] F. Kanavati et al., "Weakly-supervised learning for lung carcinoma classification using deep learning," *Sci. Rep.*, vol. 10, no. 1, p. 9297, Jun. 2020, doi: 10.1038/s41598-020-66333-x.
- [2] R. P.R., R. A. S. Nair, and V. G., "A Comparative Study of Lung Cancer Detection using Machine Learning Algorithms," in 2019 IEEE International Conference on Electrical, Computer and Communication Technologies (ICECCT), Coimbatore, India: IEEE, Feb. 2019, pp. 1–4. doi: 10.1109/ICECCT.2019.8869001.
- [3] S. S. Raoof, M. A. Jabbar, and S. A. Fathima, "Lung Cancer Prediction using Machine Learning: A Comprehensive Approach," in 2020 2nd International Conference on Innovative Mechanisms for Industry Applications (ICIMIA), Bangalore, India: IEEE, Mar. 2020, pp. 108–115. doi: 10.1109/ICIMIA48430.2020.9074947.

- [4] M. Saric, M. Russo, M. Stella, and M. Sikora, "CNN-based Method for Lung Cancer Detection in Whole Slide Histopathology Images," in 2019 4th International Conference on Smart and Sustainable Technologies (SpliTech), Split, Croatia: IEEE, Jun. 2019, pp. 1–4. doi: 10.23919/SpliTech.2019.8783041.
- [5] R. Selvanambi, J. Natarajan, M. Karuppiah, S. H. Islam, M. M. Hassan, and G. Fortino, "RETRACTED ARTICLE: Lung cancer prediction using higher-order recurrent neural network based on glowworm swarm optimization," *Neural Comput. Appl.*, vol. 32, no. 9, pp. 4373–4386, May 2020, doi: 10.1007/s00521-018-3824-3.
- [6] B. Park, H. Park, S. M. Lee, J. B. Seo, and N. Kim, "Lung Segmentation on HRCT and Volumetric CT for Diffuse Interstitial Lung Disease Using Deep Convolutional Neural Networks," *J. Digit. Imaging*, vol. 32, no. 6, pp. 1019–1026, Dec. 2019, doi: 10.1007/s10278-019-00254-8.
- [7] T. Sajja, R. Devarapalli, and H. Kalluri, "Lung Cancer Detection Based on CT Scan Images by Using Deep Transfer Learning," *Trait. Signal*, vol. 36, no. 4, pp. 339–344, Oct. 2019, doi: 10.18280/ts.360406.
- [8] S. Bhatia, Y. Sinha, and L. Goel, "Lung Cancer Detection: A Deep Learning Approach," in *Soft Computing for Problem Solving*, J. C. Bansal, K. N. Das, A. Nagar, K. Deep, and A. K. Ojha, Eds., in *Advances in Intelligent Systems and Computing*, vol. 817. Singapore: Springer Singapore, 2019, pp. 699–705. doi: 10.1007/978-981-13-1595-4\_55.
- [9] T. Ozturk, M. Talo, E. A. Yildirim, U. B. Baloglu, O. Yildirim, and U. Rajendra Acharya, "Automated detection of COVID-19 cases using deep neural networks with X-ray images," *Comput. Biol. Med.*, vol. 121, p. 103792, Jun. 2020, doi: 10.1016/j.combiomed.2020.103792.
- [10] M. Venturini, M. Cariati, P. Marra, S. Masala, P. L. Pereira, and G. Carrafiello, "CIRSE Standards of Practice on Thermal Ablation of Primary and Secondary Lung Tumours," *Cardiovasc. Intervent. Radiol.*, vol. 43, no. 5, pp. 667–683, May 2020, doi: 10.1007/s00270-020-02432-6.
- [11] T. Rahman et al., "Reliable Tuberculosis Detection Using Chest X-ray With Deep Learning, Segmentation and Visualization," *IEEE Access*, vol. 8, pp. 191586–191601, 2020, doi: 10.1109/ACCESS.2020.3031384.
- [12] S. Bharati, P. Podder, and M. R. H. Mondal, "Hybrid deep learning for detecting lung diseases from X-ray images," *Inform. Med. Unlocked*, vol. 20, p. 100391, 2020, doi: 10.1016/j.imu.2020.100391.
- [13] A. Asuntha and A. Srinivasan, "Deep learning for lung Cancer detection and classification," *Multimed. Tools Appl.*, vol. 79, pp. 7731–7762, 2020.
- [14] S. Kim, B. Rim, S. Choi, A. Lee, S. Min, and M. Hong, "Deep Learning in Multi-Class Lung Diseases' Classification on Chest X-ray Images," *Diagnostics*, vol. 12, no. 4, Art. no. 4, Apr. 2022, doi: 10.3390/diagnostics12040915.
- [15] F. Demir, A. Sengur, and V. Bajaj, "Convolutional neural networks based efficient approach for classification of lung diseases," *Health Inf. Sci. Syst.*, vol. 8, no. 1, p. 4, Dec. 2019, doi: 10.1007/s13755-019-0091-3.
- [16] P. M. Shakeel, M. A. Burhanuddin, and M. I. Desa, "Lung cancer detection from CT image using improved profuse clustering and deep learning instantaneously trained neural networks," *Measurement*, vol. 145, pp. 702–712, Oct. 2019, doi: 10.1016/j.measurement.2019.05.027.
- [17] K.-C. Chen et al., "Diagnosis of common pulmonary diseases in children by X-ray images and deep learning," *Sci. Rep.*, vol. 10, no. 1, p. 17374, Oct. 2020, doi: 10.1038/s41598-020-73831-5.
- [18] Y. Al-Issa, A. Mohammad Alqudah, H. Alquran, and A. Al Issa, "Pulmonary Diseases Decision Support System Using Deep Learning Approach," *Comput. Mater. Contin.*, vol. 73, no. 1, pp. 311–326, 2022, doi: 10.32604/cmc.2022.025750.
- [19] W. J. Sori, J. Feng, and S. Liu, "Multi-path convolutional neural network for lung cancer detection," *Multidimens. Syst. Signal Process.*, vol. 30, no. 4, pp. 1749–1768, Oct. 2019, doi: 10.1007/s11045-018-0626-9.
- [20] C. Anil Kumar et al., "Lung Cancer Prediction from Text Datasets Using Machine Learning," *BioMed Res. Int.*, vol. 2022, p. e6254177, Jul. 2022, doi: 10.1155/2022/6254177.
- [21] H. Shi, J. Lu, and Q. Zhou, "A Novel Data Augmentation Method Using Style-Based GAN for Robust Pulmonary Nodule Segmentation," in *2020 Chinese Control And Decision Conference (CCDC)*, Aug. 2020, pp. 2486–2491. doi: 10.1109/CCDC49329.2020.9164303.
- [22] G. Kasinathan, S. Jayakumar, A. H. Gandomi, M. Ramachandran, S. J. Fong, and R. Patan, "Automated 3-D lung tumor detection and classification by an active contour model and CNN classifier," *Expert Syst. Appl.*, vol. 134, pp. 112–119, Nov. 2019, doi: 10.1016/j.eswa.2019.05.041.
- [23] S. A. Althubiti, S. Paul, R. Mohanty, S. N. Mohanty, F. Alenezi, and K. Polat, "Ensemble Learning Framework with GLCM Texture Extraction for Early Detection of Lung Cancer on CT Images," *Comput. Math. Methods Med.*, vol. 2022, p. e2733965, Jun. 2022, doi: 10.1155/2022/2733965.
- [24] Q. Firdaus, R. Sigit, T. Harsono, and A. Anwar, "Lung Cancer Detection Based On CT-Scan Images With Detection Features Using Gray Level Co-Occurrence Matrix (GLCM) and Support Vector Machine (SVM) Methods," in *2020 International Electronics Symposium (IES)*, Sep. 2020, pp. 643–648. doi: 10.1109/IES50839.2020.9231663.
- [25] A. Naik and D. R. Edla, "Lung Tumor Classification Using CNN- and GLCM-Based Features," in *ICT Systems and Sustainability*, M. Tuba, S. Akashe, and A. Joshi, Eds., in *Advances in Intelligent Systems and Computing*, vol. 1270. Singapore: Springer Singapore, 2021, pp. 157–163. doi: 10.1007/978-981-15-8289-9\_15.
- [26] M. Rezaei, H. Yang, and C. Meinel, "Recurrent generative adversarial network for learning imbalanced medical image semantic segmentation," *Multimed. Tools Appl.*, vol. 79, no. 21, pp. 15329–15348, Jun. 2020, doi: 10.1007/s11042-019-7305-1.